A Method for Accurate Road Centerline Extraction From a Classified Image

Zelang Miao, Bin Wang, Wenzhong Shi, and Hao Wu

***Abstract*—Accurate road centerline extraction plays an important role in practical remote sensing applications. Most existing centerline extraction methods have many limitations when the classified image contains complicated objects such as curvilinear, close, or short extent features. To cope with these limitations, this study presents a novel accurate centerline extraction method that integrates tensor voting, principal curves, and the geodesic method. The proposed method consists of three main steps. Tensor voting is first used to extract feature points from the classified image. The extracted feature points are then projected onto the principal curves. Finally, the feature points are linked by the geodesic method to create the central line. The experimental results demonstrate that the proposed method, which is automatic, provides a comparatively accurate solution for centerline extraction from a classified image.**

***Index Terms*—Accurate centerline extraction, classified images, geodesic method, principal curves, tensor voting.**

I. Introduction

HIGH-RESOLUTION satellite sensors, such as WorldView-2, SPOT, and IKONOS, have many applications. Road centerlines extracted from remote sensing images in many remote sensing applications have been widely used in transportation database updating, urban planning, vehicle navigation, etc. Various approaches have been developed over the past decades to address the road extraction issue. Mena [1] and Das *et al.* [2] have compiled good reviews on road extraction methods and a comprehensive comparison of different road extraction methods was given by Mayer *et al.* [3]. Existing road extraction methods can be categorized into three main groups: 1) *pixel-based*, 2) *region-based*, and 3) *knowledge-based* [4]. Specifically, *region-based* methods are an important class of road extraction algorithms that mainly consist of two stages. The first stage of a *region-based* method is the road classification/segmentation stage, which has been well-researched and many related methods have been developed. Hinz and Baumgartner [5] proposed an automatic method for urban road networks extraction from multi-view aerial imagery by integrating road models and context information. Price [6] proposed a method concentrated on urban street grid description and verification. Chaudhuri *et al.* proposed integrating directional morphological enhancement and segmentation techniques to detect a road from high-resolution satellite images [7]. Senthilnath *et al.* [8] combined the structural, spectral, and geometric characteristics of roads for automatic road extraction for urban regions. Yuan *et al.* [9] automatically extracted the road network using the locally excitatory globally inhibitory oscillator networks (LEGION) segmentation method. Rajeswari *et al.* [10] presented an automatic road extraction method that integrated the strengths of level set, normalized cuts, and mean-shift methods. Similarly, incorporating multiple features of roads has been used to delineate road features [11]–[14]. Senthilnath *et al.* [15] also extracted linear features (i.e., a river) from multi-temporal MODIS images by fusing image classification and segmentation results.

The second stage of a *region-based* method extracts the centerlines from the classified images. The commonly used method is the thinning algorithm [16]. Although the thinning algorithm is efficient in implementation, it always produces many spurs that reduce the centerline smoothness and correctness. To extract accurate centerlines, a Radon transform was applied to extract centerlines from the classified image [17]. This method shows a good performance when dealing with straight road segments. However, it is not suitable for short and curvilinear lines. Poullis and You [4] used the Hough transform to extract road centerlines. This approach uses a set of Gaussian-based filters to compute the magnitude of the road pixels. The Hough transform is subsequently implemented to extract the road centerlines in an iterative manner. Although this approach reports a good performance, some false positives exist due to the limitations of the Hough transform. A self-organized clustering method was developed by Doucette *et al.* [18] for road centerline extraction from classified images. This approach cannot extract centerlines located at the end of road segments. Therefore, accurate road centerline extraction from a classified image still has not been clearly resolved. Thus, the objective of this study is to determine how to extract smooth and accurate road centerlines from classified images.

Some studies have focused on road extraction from different perspectives. Ünsalan and Sirmaçek [19] used probabilistic and graph theoretical methods to extract road networks. Their method relies on edge information. To solve the gap closure issue, higher-order active contour energies were investigated [20]. Poz *et al.* [21] used stereoscopic aerial images in object-space to

Manuscript received August 03, 2013; revised February 15, 2014; accepted February 28, 2014. Date of publication March 30, 2014; date of current version January 21, 2015. This work was supported in part by the National Natural Science Foundation of China (41201451 and 40901214), in part by Ministry of Science and Technology of China (Project no.: 2012BAJ15B04 and 2012AA12A305), in part by Research Grants Council, Hong Kong (PolyU 5249/12E), and in part by Hong Kong Polytechnic University (Project no.: 1-ZVBA, G-U753, G-YK75, and G-YJ75). The work of B. Wang is supported by doctoral grant from the AXA Research Fund.

Z. Miao, B. Wang, and W. Shi are with the Department of Land Surveying and Geo-Informatics, Hong Kong Polytechnic University, Hong Kong, China (e-mail: lswzshi@polyu.edu.hk).

Z. Miao is also with School of Environmental Science and Spatial Informatics, China University of Mining and Technology, Xuzhou 221116, China.

H. Wu is with School of Resources and Environmental Engineering, Wuhan University of Technology, Wuhan 430070, China.

Color versions of one or more of the figures in this paper are available online at http://ieeexplore.ieee.org.

Digital Object Identifier 10.1109/JSTARS.2014.2309613

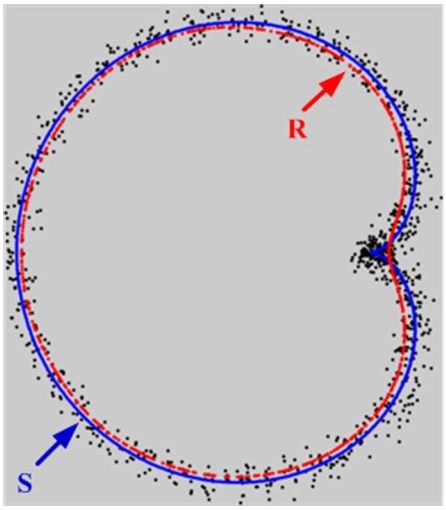

Fig. 1. Example of centerline extraction using SCMS.

extract roads in rural areas. Particle filtering and extended Kalman Filtering were used to extract roads from satellite images [22]. This method relied on road seed points that had to be provided by users. Based on the Fourier shape descriptor, Hu *et al.* [23] proposed a concept of road footprints to measure the probability that a pixel is located on a road. A road tree is then constructed to formulate the road network. In addition to the optical satellite images, some authors also extracted roads from SAR imagery [24], [25].

In the field of machine learning and computer vision, principal curves and smooth curves passing through data points [26] have been investigated. From the description of principal curves, it is evident that this method could be a preferable choice for extracting centerlines. Recently, Ozertem and Erdogmus [27]–[29] proposed a practical method, called the subspace constrained mean shift (SCMS) method, to extract a smooth centerline from noisy points. The SCMS method projects all of the input data points to the closest ridge of the probability density function (pdf) generated by the kernel density estimation (KDE). The results produced by SCMS are smooth and robust. However, SCMS has to iteratively project all of the points to principal curves, and hence the computation load is very high, which limits its applications. In addition, SCMS is a biased estimator [30]. Fig. 1 shows an example of centerline extraction using SCMS. In Fig. 1, the black dots denote the point cloud, the blue line denotes the true centerline S, and the dashed red circle is the estimated centerline R detected by SCMS. It can be seen that R is a biased surrogate for S, which indicates that SCMS is a biased estimator. Generally, the bias will severely influence the accuracy of the centerline. This study proposes a framework for extracting a centerline from a classified image that integrates the strengths of tensor voting, SCMS, and the geodesic method. Unlike SCMS, the proposed method only needs to project a few feature points onto principal curves. Furthermore, the centerline extracted by the proposed method is unbiased. Details of the proposed method are introduced in Section II.

The remainder of this paper is organized as follows. The new approach is presented in Section II. The experimental results are given and discussed in Section III. Finally, Section IV concludes the paper.

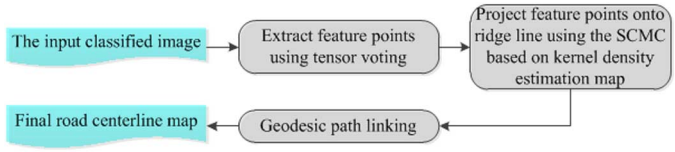

Fig. 2. Flowchart of the proposed method.

II. Methodology

This study devises a computationally efficient approach to extract accurate centerlines from classified images. Fig. 2 summarizes the proposed method.

The proposed method consists of the three following steps.

1) Feature points (i.e., junction and end points) are first extracted from the classified image.
2) The probability of each pixel being located on the road centerline is computed using the KDE method. Subsequently, the feature points are projected onto ridge lines using the SCMS method.
3) The projected feature points are linked by the geodesic method to create the central line to formulate the road network.

The details of each step are described in Section II-A.

A. Tensor Voting

The first step of the proposed method is to use tensor voting to extract the feature points from the classified image. Tensor voting is a perceptual grouping and segmentation framework introduced by Medioni *et al.* [31], [32]. Let T denote a second-order symmetric tensor for a 2-D case that is defined as

$$T = \begin{bmatrix} I_x^2 & I_x I_y \\ I_x I_y & I_y^2 \end{bmatrix} \tag{1}$$

where I_x and I_y denote the partial derivative of image I along the x-axis and y-axis, respectively. In this study, the Sobel operator [16] is selected to compute the partial derivatives of the image. Eigen-decomposition is subsequently applied to the tensor matrix T as follows:

$$\begin{aligned} T &= \begin{bmatrix} \overrightarrow{e_1} & \overrightarrow{e_2} \end{bmatrix} \begin{bmatrix} \lambda_1 & 0 \\ 0 & \lambda_2 \end{bmatrix} \begin{bmatrix} \overrightarrow{e_1} \\ \overrightarrow{e_2} \end{bmatrix} \\ &= \lambda_1 \overrightarrow{e_1}\overrightarrow{e_1}^T + \lambda_2 \overrightarrow{e_2}\overrightarrow{e_2}^T \end{aligned} \tag{2}$$

where λ_i are eigenvalues with the ordering $\lambda_1 \geq \lambda_2$ and $\overrightarrow{e_i}$ represents the corresponding eigenvectors.

The tensor matrix T can be rewritten as

$$T = (\lambda_1 - \lambda_2)\overrightarrow{e_1}\overrightarrow{e_1}^T + \lambda_2\left(\overrightarrow{e_1}\overrightarrow{e_1}^T + \overrightarrow{e_2}\overrightarrow{e_2}^T\right) \tag{3}$$

where $\overrightarrow{e_1}\overrightarrow{e_1}^T$ is a stick tensor with associated saliency $(\lambda_1 - \lambda_2)$, which indicates an elementary curve, $(\overrightarrow{e_1}\overrightarrow{e_1}^T + \overrightarrow{e_2}\overrightarrow{e_2}^T)$ with

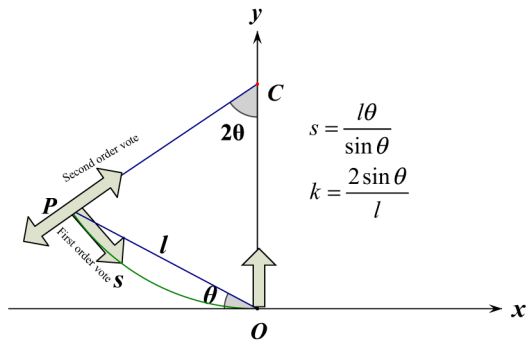

Fig. 3. Votes cast by a stick tensor located at the origin O. C is the center of the osculating circle passing through points P and O.

associated saliency λ_2 describes a structure that has no orientation preference to a location where multiple orientations coexist.

The saliency decay function, as shown in Fig. 3, can be expressed as

$$DF(s,\kappa,\sigma) = e^{-\left(\frac{s^2+c\kappa^2}{\sigma^2}\right)} \tag{4}$$

where s is the arc length of OP, κ is the curvature, c controls the degree of decay with curvature, and σ is the scale factor that determines the effective neighborhood size. The scale factor σ is determined as follows:

$$\sigma = 3w_R \tag{5}$$

where w_R denotes the mean road width.

Based on the saliency decay function, the second-order tensor voting for the 2-D case is defined as

$$\mathrm{S}_{SO}(d,\theta) = DF(s,\kappa,\sigma)\begin{bmatrix} -\sin(2\theta) \\ \cos(2\theta) \end{bmatrix}[-\sin(2\theta) \quad \cos(2\theta)]. \tag{6}$$

The first order tensor voting for the 2-D is defined as

$$\mathrm{S}_{SO}(d,\theta) = DF(s,\kappa,\sigma)\begin{bmatrix} -\cos(2\theta) \\ -\sin(2\theta) \end{bmatrix}. \tag{7}$$

After tensor voting, vote analysis is performed to extract two types of feature points: 1) junction points and 2) end points. Feature points are classified based on the following two rules.

1) Points that satisfy $\lambda_1 \approx \lambda_2 > 0$ are classified as region or junction points.
2) The local maxima of polarity are detected as endpoints. The local maxima are the points within a given neighborhood at which the pixel takes the largest value. The image dilation [16], one of mathematical morphology operations, can be applied to detect local maxima.

An example of feature point extraction using tensor voting is presented in Fig. 4. As can be seen from Fig. 4(b), feature points extracted by tensor voting are areas, not single points. In this study, centroids of these areas are taken as feature points, resulting in Fig. 4(c).

After the extraction of feature points, the corresponding connectivity matrix is constructed using Algorithm 1. The

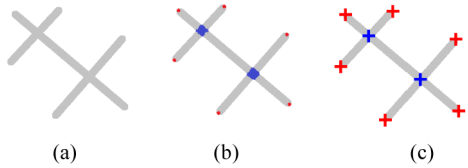

Fig. 4. (a) Input image. (b) Feature points extraction results using tensor voting, where junction points are shown in blue and end points in red. (c) Centroids of the junction points are shown in blue crosses and end points in red crosses.

connectivity matrix of each connected component (CP) can be defined as follows: a feature point is connected to any feature points except itself. In this means, if some junctions are missed, they can still be recovered when the algorithm tries to link endpoints. Another advantage of introducing this connectivity matrix is that, for each end point, there is no necessary to determine which junction point is connected to, thereby resulting in an efficient way of constructing such connectivity matrix. Meanwhile, Fig. 5 shows an example of generating the connectivity matrix from foregoing extracted feature points. The feature points detected by the tensor voting are shown in Fig. 5(a), and the corresponding connectivity matrix is shown in Fig. 5(b). As can be seen, the connectivity matrix is symmetric, and hence only the lower triangular elements need to be processed by the following procedures.

Algorithm 1 The connectivity matrix construction algorithm

1. Perform connected component analysis (CCA) [16] on the classified image.
2. Select one connected component $comp_i$ and then perform tensor voting to extract feature points. Suppose the component contains M_i feature points (i.e., junction points and end points).

   for $m_1 = 1, \ldots, M_i$

   for $m_2 = 1, \ldots, M_i$ and $m_2 \neq m_1$

   $Conn(m_1 m_2) = 1$

   end for

   end for
3. Repeat Step 2 until all of the components are analyzed.

B. Principal Curves

Although the feature points extracted in Fig. 5(a) do not precisely locate on the centerline, principal curves can be applied to project these coarse feature points to ridge lines, and thus precise feature points can be obtained. Given a d-variate random sample $X_1, X_2, \ldots, X_n$ drawn from a density function f, the kernel density estimator is defined as

$$\hat{f}\left(x;\sum\right) = n^{-1}\sum_{i=1}^{n} K_{\sum}(x - X_i) \tag{8}$$

where $x = (x_1, x_2, \ldots, x_d)^{\mathrm{T}}$ and $X_i = (X_{i1}, X_{i2}, \ldots, X_{id})^{\mathrm{T}}$, $i = 1, 2, \ldots, n$. In addition, $\sum$ is a symmetric positive definite

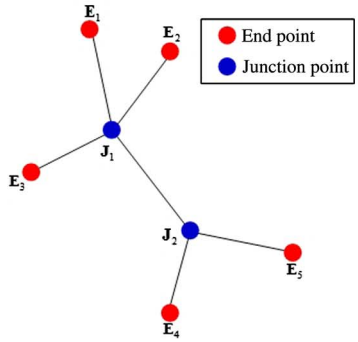

(a)

	J1	J2	E1	E2	E3	E4	E5
J1	0	1	1	1	1	1	1
J2	1	0	1	1	1	1	1
E1	1	1	0	1	1	1	1
E2	1	1	1	0	1	1	1
E3	1	1	1	1	0	1	1
E4	1	1	1	1	1	0	1
E5	1	1	1	1	1	1	0

(b)

Fig. 5. Example of constructing the connectivity matrix. (a) Feature points extracted by tensor voting. (b) The corresponding connectivity matrix.

$d \times d$ matrix called the bandwidth matrix, which is crucial in determining the performance of $\hat{f}$. K is a d-variate kernel function that is defined as

$$K_{\sum}(x) = \left|\sum\right|^{-1/2} K\left(\sum^{-1/2} x\right) \tag{9}$$

where $|\cdot|$ stands for the determinant of $\sum$ and K satisfies $\int K(x)dx = 1$, where the integral is regarded as being over R^d unless stated otherwise. Here, we take $K(x) = (2\pi)^{-d/2}\exp(-\frac{1}{2}x^{\mathrm{T}}x)$, the standard normal throughout, which is a common choice during many kernel estimation functions.

We choose the bandwidth matrix $\sum^{-1} = n^{\frac{2}{d+4}}\hat{\sum}^{-1}$ by generalizing Scott's rule of thumb. For details of this empirical formula, please refer to Ahamada and Flachaire [33]. Note the difference between the symbols, as one is the sample covariance and the other is the sample standard deviation matrix. The kernel density estimator is constructed above as

$$p\left(x;\sum\right) = \frac{1}{n(2\pi)^{d/2}|\sum|^{1/2}} \bullet \sum_{i=1}^{n} \exp\left(-\frac{1}{2}(x - X_i)^{\mathrm{T}}\sum^{-1}(x - X_i)\right). \tag{10}$$

To better solve the principle curve, we take the logarithm of the density function $p(x;\sum)$

$$f(p(x)) = \log(p(x)). \tag{11}$$

The gradient and Hessian matrices for KDE are

$$g_f(x) = f'(p(x))\nabla p(x)^{\mathrm{T}} = p(x)^{-1}g(x) \tag{12}$$

$$\begin{aligned} H_f(x) &= f''(p(x))\nabla p(x)^{\mathrm{T}}\nabla p(x) + f'(p(x))\nabla^2 p(x) \\ &= f''(p(x))g(x)g(x)^{\mathrm{T}} + f'(p(x))H(x) \\ &= -p(x)^{-2}g(x)g(x)^{\mathrm{T}} + p(x)^{-1}H(x). \end{aligned} \tag{13}$$

Based on previous formulas, the fixed-point update rule can be written as

$$m_{\sum}(x) = \frac{\sum_{i=1}^{n}\exp\left(-\frac{1}{2}(x - X_i)^{\mathrm{T}}\sum^{-1}(x - X_i)\right)X_i}{\sum_{i=1}^{n}\exp\left(-\frac{1}{2}(x - X_i)^{\mathrm{T}}\sum^{-1}(x - X_i)\right)} - x. \tag{14}$$

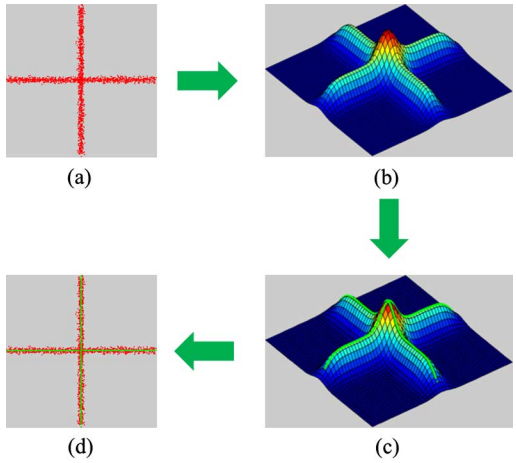

Fig. 6. Example of a principal curve. (a) Noisy input points. (b) The estimated probability density map. (c) The principal curve over the probability density map, where the principal curve is shown in green. (d) The principal curve projected back onto the plane of original points.

This iteration rule is similar to that of the mean-shift algorithm and thus it is named the subspace constrained mean shift (SCMS) method, which is summarized in Algorithm 2. An example of projecting points onto the ridge line is illustrated in Fig. 6.

Algorithm 2 Subspace constrained mean shift method

1. Bandwidth selection (i.e., the kernel covariance).
2. For every trajectory, proceed from each sample with the projected mean shift iteration, such as $x_t = x_i$, conduct the eigenvalue decomposition of $H_f(x)$, and construct the orthogonal projector matrix $P = I - qq^{\mathrm{T}}$, here q is an eigenvector corresponding to the eigenvalue with a smaller absolute value.
3. Check whether the iteration step satisfies the termination criterion e_{thre}. If $s = Pm_{\sum}(x) < e_{thre}$, stop; else set $x_{t+1} = x_t + s$ and return to Step 2.

C. The Geodesic Method

After the projection of feature points onto principal curves in Fig. 6(b), the geodesic method [34] is subsequently used to create the central line by linking the feature points. Consider a smooth curve $r : [0, 1] \rightarrow \Omega$ on an image, where Ω is the image domain

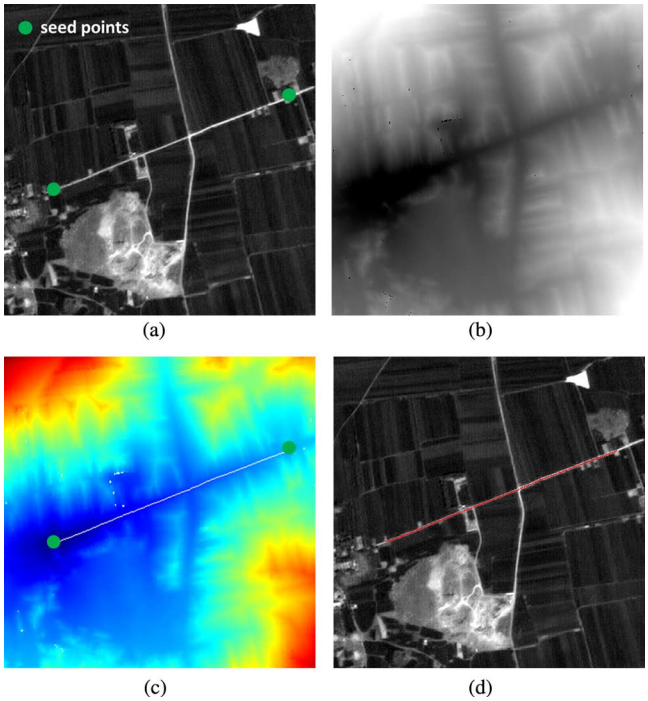

Fig. 7. Example of feature points linking using the geodesic method. (a) The original image. (b) The weight image. (c) The geodesic distance and the minimal path. (d) The superposition result of the original image and the road centerline extracted by the geodesic method.

that is defined as $\Omega = [0,1]^2$. The smooth curve γ is generally constrained as

$$\{\gamma : [0,1] \to \Omega \backslash \gamma(0) = x_s \ and \ \gamma(1) = x_e\} \tag{15}$$

where x_s and x_e denote the starting point and ending point, respectively.

Let $L(\gamma)$ denote the weighted length of the smooth curve γ. The weighted length $L(\gamma)$ can be computed as follows:

$$L(\gamma) = \int_0^1 W(\gamma(t)) \|r'(t)\| dt \tag{16}$$

where $\gamma'(t) \in \mathbb{R}^2$ is the derivative of γ, and t denotes the parameter of the curve.

Let $f : \Omega \to \mathbb{R}$ denote the probability density estimation map that is generated by KDE. For the purpose of road network formulating, a road can be approximately defined as a smooth curve that has a constant kernel density value $c \in \mathbb{R}$. Based on this definition of a road model, a weight function $W(x)$ can be defined as

$$W(x) = |f(x) - c| + \varepsilon \tag{17}$$

where ε (i.e., $\varepsilon = 0.01$) is a small value that prevents $W(x)$ from vanishing. In this study, the constant value c is fixed to $c = f(x_e)$. As can be seen from (17), this is the area where the principal curve (i.e., the road centerline) is passing through the area that has low weights.

The minimal path that links two feature points is a global minimizer of the length that should satisfy the following equation

$$\gamma^* = \arg\min_{\gamma \in (x_s, x_e)} L(\gamma). \tag{18}$$

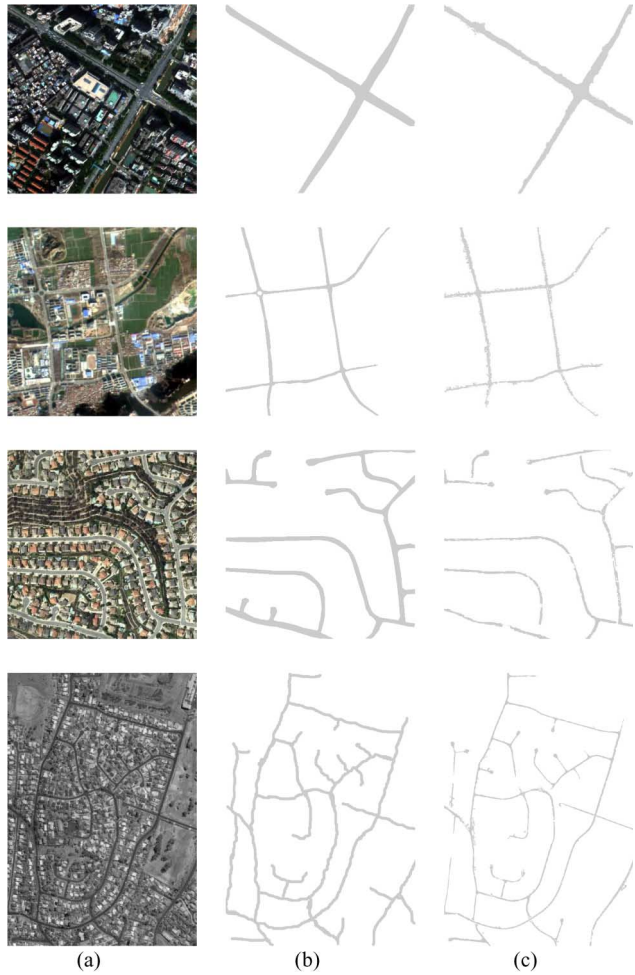

Fig. 8. (a) Original remote sensing images. (b) Ground truth data sets. (c) Classification results.

The steps of the feature points linking procedure based on the geodesic method are presented in Algorithm 3. Fig. 7 shows an example of feature points linking using the geodesic method.

Algorithm 3 Feature points linking using the geodesic method

1. Compute the kernel density estimation map of the classified image.
2. Extract road feature points using tensor voting.
3. Construct the weight matrix using Equation (17).
4. Construct the geodesic distance map and find the geodesic path.
5. Link feature points using the geodesic path.

III. Experiments

In this section, several experiments that test the proposed method are described. The proposed method is also compared with other methods in the literature to show the advantages and disadvantages of the proposed method.

TABLE I
CLASSIFICATION ACCURACIES OF THE FOUR TEST IMAGES

Experiment	Classification accuracy (%)	Error rate (%)
1	87.04	12.96
2	84.00	16.00
3	72.59	27.41
4	51.30	48.70

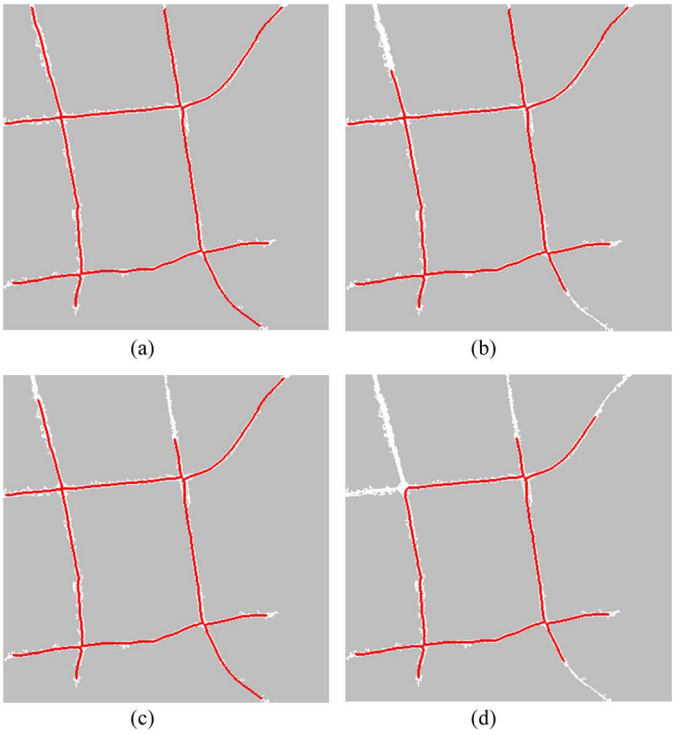

Fig. 9. (a)–(d) show the centerline extraction result for the scale parameters 3, 5, 7, and 9, respectively. The extracted centerlines are shown in red for display.

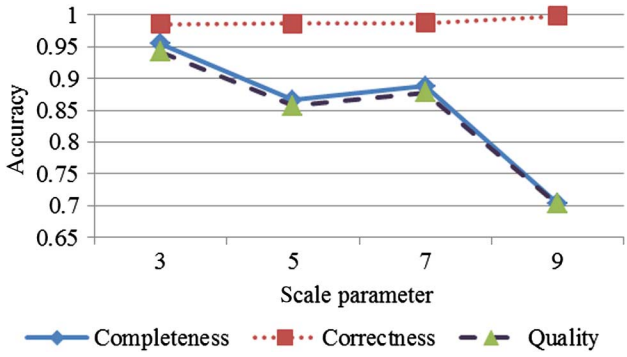

Fig. 10. Evaluation results of the influence of scale parameter on road centerline extraction accuracy.

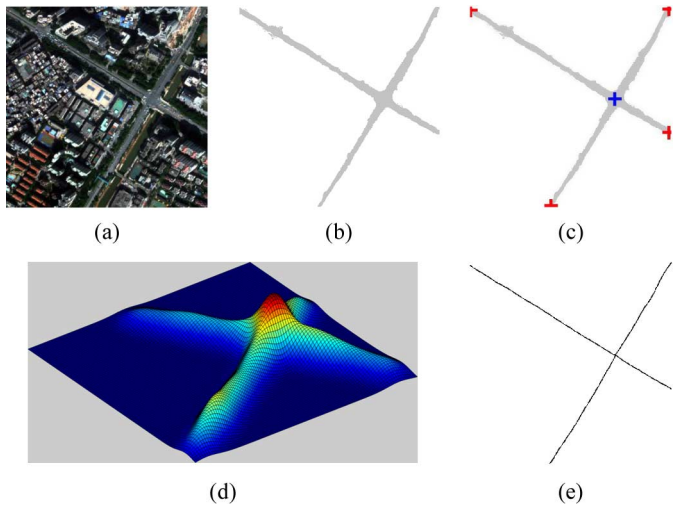

Fig. 11. Results of the first experiment. (a) The original image. (b) The classified road map. (c) Feature points extracted by tensor voting, junction points are shown as blue crosses, and end points as red crosses. (d) Probability density estimation result of the classified road map. (e) Road centerline extraction result.

A. Classification

In this paper, the method proposed by Shi *et al.* [13] is selected to classify the satellite image. This method integrates the strengths of spectral-spatial classification, local spatial statistics, information fusion, and road shape features, and generally achieves relatively higher classification accuracy than other classification methods. Fig. 8 depicts the classification results for four satellite images. Columns (a)–(c) of Fig. 8 are test images, ground truth data sets, and classification results, respectively. In this study, the first three ground truth data sets are generated with a hand drawing method and the last one is provided by Dr. C. Ünsala from Yeditepe University. The classification accuracy and error rate [35] are used to evaluate the accuracies of the classification results that are listed in Table I. It is worth mentioning that classification accuracy is not equal to road extraction accuracy, as their evaluation methods are totally different.

As can be observed from Table I, the classification method achieves comparable satisfactory results for the four satellite images. However, the method fails to extract some roads due to the complexity of the natural scene, image noises, and limitations of the classification methods. Although the classification procedure can rarely produce ideal results that cover the whole road network, it provides an initial result that can reduce the amount of manual work necessary and improve the efficiency of the road extraction procedure.

B. Tests of Parameters

The proposed method only has one parameter that needs to be set by users: the scale parameter σ. In this experiment, Fig. 8(b) is selected as the test image. Here, the value of σ is changed from 3 to 9 and the effect on the road centerline detection performance is observed. The results are provided in Fig. 9. Three accuracy measures proposed by Wiedemann *et al.* [36] are used to quantitatively evaluate the road centerline extraction accuracy

$$E_1 = \frac{TP}{TP + FN} \tag{19}$$

$$E_2 = \frac{TP}{TP + FP} \tag{20}$$

$$E_3 = \frac{TP}{TP + FP + FN} \tag{21}$$

where E_1, E_2, and E_3 denote completeness, correctness, and quality, respectively. TP, FN, and FP represent true positive, false negative, and false positive, respectively.

Fig. 12. Results of the second experiment. (a) The original image. (b) The classified road map. (c) Road centerline extraction result.

Fig. 13. Results of the third experiment. (a) The original image. (b) The classified road map. (c) Road centerline extraction result.

Fig. 14. Results of the fourth experiment. (a) The original image. (b) The classified road map. (c) Road centerline extraction result.

Fig. 10 gives the quantitative evaluation result. As can be seen, the scale parameter has a small effect on the correctness, indicating that the proposed method can always produce correct road centerlines. It can also be observed that as the value of the scale parameter exceeds 3, the road centerline accuracy decreases, because when the scale parameter is large, tensor voting will start to "cross-talk" too much and this leads to the elimination of some feature points. Therefore, the scale parameter is fixed to 3 in this study to guarantee extraction accuracy.

C. Experiments

In the first experiment, the proposed method was tested on a WorldView-2 satellite image. The test image has a spatial size of 400×400 pixels, with 11578 of them representing the classified road map. Fig. 11(a) (b) show the original satellite image and its corresponding classified road map. Feature points were first extracted from the classified road map using tensor voting, as shown in Fig. 11(c). The KDE was then used to generate the probability density estimation map, resulting in Fig. 11(d). As can be seen in Fig. 11(d), road centerlines were located on the principal curve of the probability density estimation map. Feature points (one junction point and four end points) were then projected onto the principal curve using the SCMS method. Finally, the geodesic method was performed to link the end points and junction point. Fig. 11(e) shows the road centerline extraction result produced by the proposed method.

Another satellite image was picked to test the proposed method. The test image was recorded at *Xuzhou City*, China, by the ZiYuan-3 satellite, a Chinese Earth Observation satellite. Fig. 12(a) gives the test image, which has a spatial size of 400×400 pixels. The classified image has 8009 road pixels, as shown in Fig. 12(b). The road centerline extracted by the proposed method is given in Fig. 12(c).

In the third case study, the developed method was tested on a QuickBird image downloaded from [37]. The image has a spatial size of 512×512 pixels, as shown in Fig. 13(a). It can be observed that roads in this image have many branches, which is a very common pattern in real world applications. The classified road map, as shown in Fig. 13(b), has 16503 road points. The road centerline extraction result is shown in Fig. 13(c).

In the fourth case study, the developed method was tested on a GeoEye-1 image provided by Dr. C. Ünsalan. Fig. 14(a) shows the test image, which has a spatial size of 986×682 pixels. In this study, the test image includes different types of junctions, such as a "T" junction, "+" junction, and "L" junction. The test area also contains different widths of roads. Therefore, the test image is very complicated. The classified road map, as shown in Fig. 14(b), has 35177 road points. The road centerline extraction result is shown in Fig. 14(c). As can be seen, the proposed method still showed good performance, even when the classified road map was complicated.

D. Comparisons With the Existing Methods

In this section, the proposed method is compared with the thinning algorithm and SCMS. In this study, MATLAB was used as the coding environment on a PC that has an Intel Core2Quad processor with 2.83-GHz clock speed. The results of the thinning algorithm are presented in Fig. 15(a), of SCMS in Fig. 15(b), and of the proposed method in Fig. 15(c). As can be observed from the results of the three centerline extraction methods, both SCMS and the proposed method can provide smoother results than the thinning algorithm. There are many undesired spurs and loops in the thinning algorithm results. Although SCMS can solve some of the limitations of the thinning algorithm, its performance is still poorer in general. Specifically, in the third and fourth test images, there are obvious biases and phase transitions [30]. With the proposed method, there are no spurs, bias, or phase transitions. This visual comparison evidently validates the advantages of the proposed method in road centerline extraction from classified images.

The three methods were also compared in terms of both the computation complexity and accuracy. Table II shows the results of the comparison of the computation complexity of the three methods on the four classified images. As can be seen, the thinning algorithm achieves a higher computational efficiency than SCMS and the proposed method. The experimental results also indicate that the proposed method is more efficient than SCMS. This is particularly true when the topological structure of the classified image is simple. The accuracy results of the three road centerline extraction methods are listed in Table III. It can be seen that the proposed method achieves the highest accuracy, whereas SCMS shows the worst performance among the three methods. This is mainly due to the fact that when the structure of the classified image is complicated, it is difficult to obtain satisfactory bandwidth estimation. An inadequate bandwidth will lead to over-smoothing (i.e., bias) or under-smoothing (i.e., phase transition). Both over-smoothing and under-smoothing significantly reduce the accuracy of SCMS. Table III also indicates that the thinning algorithm will produce many undesired spurs that reduce the centerline extraction accuracy and the smoothness. By contrast, both SCMS and the proposed method have no spurs, and hence retain the centerline smoothness.

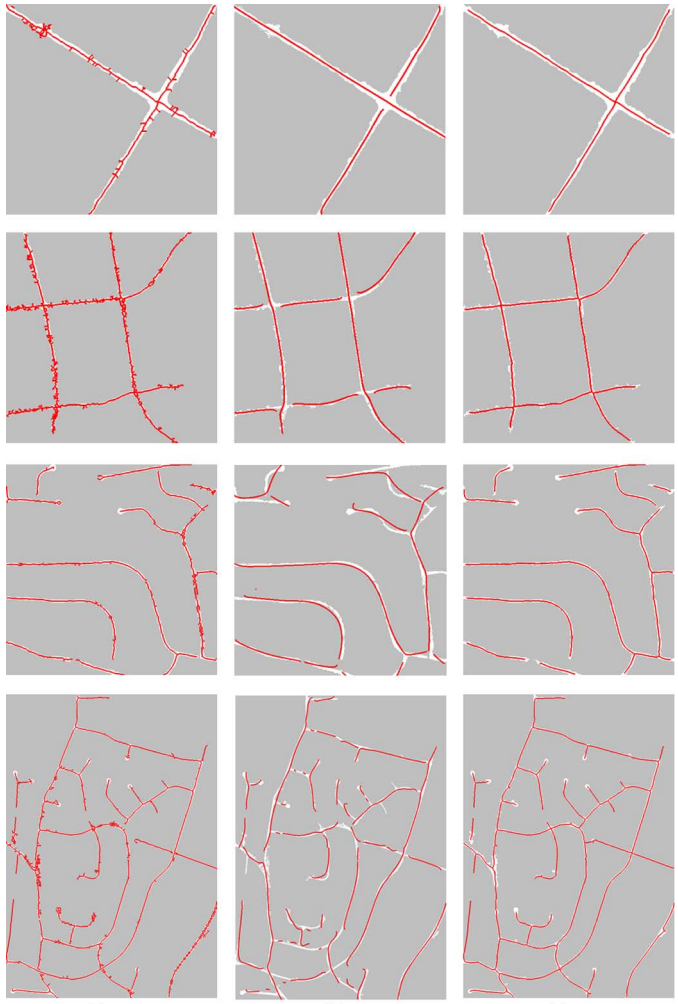

Fig. 15. Comparison results of different road centerline extraction methods. (a) Results of the thinning algorithm. (b) Results of SCMS. (c) Results of the proposed method. The centerlines are shown in red for display.

TABLE II
COMPARISON OF COMPUTATION TIME FOR DIFFERENT CENTERLINE EXTRACTION METHODS

Experiment	Number of points	Computation time (s)		
		The thinning algorithm	SCMS	The proposed method
1	11578	0.20	58.77	2.18
2	8009	0.07	35.73	1.97
3	16503	0.99	172.99	67.93
4	35177	1.02	1142.95	73.48

TABLE III
QUANTITATIVE EVALUATION OF DIFFERENT CENTERLINE EXTRACTION METHODS

Method	Experiment 1			Experiment 2		
	E_1 (%)	E_2 (%)	E_3 (%)	E_1 (%)	E_2 (%)	E_3 (%)
Thinning	**97.19**	89.74	87.47	**97.34**	92.55	90.27
SCMS	95.95	98.32	94.40	81.46	87.45	72.93
proposed	96.57	**99.74**	**96.33**	95.47	**98.60**	**94.20**
Method	Experiment 3			Experiment 4		
	E_1 (%)	E_2 (%)	E_3 (%)	E_1 (%)	E_2 (%)	E_3 (%)
Thinning	**89.04**	88.77	80.02	**76.24**	68.54	56.48
SCMS	35.78	44.43	24.72	47.54	59.14	35.78
proposed	84.34	**96.10**	**81.55**	73.47	**75.08**	**59.07**

From the above discussion, it can be concluded that the proposed method achieves the best balance between accuracy and the computational complexity among these three methods. Thus, the proposed method is more practical for accurate and efficient road centerline extraction from classified images.

IV. CONCLUSION

This study presents an automatic approach for 2-D road centerline extraction from classified satellite images. In particular, the proposed method incorporates the strengths of tensor voting, the SCMS method, and the geodesic method. The proposed method is a three-stage procedure in which feature points are first identified using tensor voting. In the second stage, the SCMS method is applied to project feature points onto the principal curve. Finally, the feature points are linked by the geodesic method to create the central lines, which form the road centerline network.

The proposed method was compared with the widely used SCMS and the thinning algorithm methods. The experimental results indicate that both the proposed method and SCMS do not produce spurs and retain smoother centerlines than the thinning algorithm. The results also indicate that the proposed method solves the limitations of SCMS. In contrast to SCMS, the proposed method can achieve unbiased centerlines with higher computational efficiency. It can be concluded that the proposed method provides a practical solution for accurate and efficient road centerline delineation from classified images.

In the presented form, the proposed method cannot process segments with a closed form (i.e., a circle). Our future research will focus on processing segments with a closed form using the piece-wise method.

ACKNOWLEDGMENT

The authors would like to thank Prof. P. Gamba from the University of Pavia for his kind discussion on road junction extraction, Prof. D. Erdogmus from Northwestern University for his kind help on the subspace constrained mean shift method, and Dr. C. Ünsala from Yeditepe University for kindly providing GeoEye-1 images. The authors would also like to thank the Editor and anonymous Reviewers whose valuable comments have greatly improved this paper.

REFERENCES

[1] J. B. Mena, "State of the art on automatic road extraction for GIS update: A novel classification," *Pattern Recognit. Lett.*, vol. 24, no. 16, pp. 3037–3058, Dec. 2003.
[2] S. Das, T. T. Mirnalinee, and K. Varghese, "Use of salient features for the design of a multistage framework to extract roads from high-resolution multispectral satellite images," *IEEE Trans. Geosci. Remote Sens.*, vol. 49, no. 10, pp. 3906–3931, Oct. 2011.
[3] H. Mayer, S. Hinz, U. Bacher, and E. Baltsavias, "A test of automatic road extraction approaches," *Int. Arch. Photogramm. Remote Sens. Spatial Inf. Sci.*, vol. 36, no. 3, pp. 209–214, 2006.
[4] C. Poullis and S. You, "Delineation and geometric modeling of road networks," *ISPRS-J. Photogramm. Remote Sens.*, vol. 65, no. 2, pp. 165–181, Mar. 2010.
[5] S. Hinz and A. Baumgartner, "Automatic extraction of urban road networks from multi-view aerial imagery," *ISPRS-J. Photogramm. Remote Sens.*, vol. 58, no. 1–2, pp. 83–98, Jun. 2003.
[6] K. Price, "Urban street grid description and verification," in *Proc. 5th IEEE Workshop Appl. Comput. Vision,* 2000, pp. 148–154.
[7] D. Chaudhuri, N. K. Kushwaha, and A. Samal, "Semi-automated road detection from high resolution satellite images by directional morphological enhancement and segmentation techniques," *IEEE J. Sel. Topics Appl. Earth Observ. Remote Sens.*, vol. 5, no. 5, pp. 1538–1544, Oct. 2012.
[8] J. Senthilnath, M. Rajeswari, and S. N. Omkar, "Automatic road extraction using high resolution satellite image based on texture progressive analysis and normalized cut method," *J. Indian Soc. Remote Sens.*, vol. 37, no. 3, pp. 351–361, Sep. 2009.
[9] J. Yuan, D. Wang, B. Wu, L. Yan, and R. Li, "LEGION-based automatic road extraction from satellite imagery," *IEEE Trans. Geosci. Remote Sens.*, vol. 40, no. 2, pp. 4528–4538, Nov. 2011.
[10] M. Rajeswari, K. S. Gurumurthy, S. N. Omkar, J. Senthilnath, and L. P. Reddy, "Automatic road extraction using high resolution satellite images based on level set and mean shift methods," in *Proc. 3rd ICECT,* Kanyakumari, India, 2011, pp. 424–428.
[11] Z. Miao, W. Shi, H. Zhang, and X. Wang, "Road centerline extraction from high-resolution imagery based on shape features and multivariate adaptive regression splines," *IEEE Geosci. Remote Sens. Lett.*, vol. 10, no. 3, pp. 583–587, May 2013.
[12] W. Shi, Z. Miao, and D. Johan, "An integrated method for urban main road centerline extraction from optical remotely sensed imagery," *IEEE Trans. Geosci. Remote Sens.*, vol. 52, no. 6, pp. 3359–3372, Jul. 2013.
[13] W. Shi, Z. Miao, Q. Wang, and H. Zhang, "Spectral-spatial classification and shape features for urban road centerline extraction," *IEEE Geosci. Remote Sens. Lett.*, vol. 11, no. 4, pp. 788–792, Apr. 2014.
[14] X. Huang and L. Zhang, "Road centerline extraction from high-resolution imagery based on multiscale structural features and support vector machines," *Int. J. Remote Sens.*, vol. 30, no. 8, pp. 1977–1987, Apr. 2009.
[15] J. Senthilnath, S. Bajpai, S. N. Omkar, P. G. Diwakar, and V. Mani, "An approach to multi-temporal MODIS image analysis using image classification and segmentation," *Adv. Space Res.*, vol. 50, no. 9, pp. 1274–1287, Nov. 2012.
[16] R. C. Gonzalez, R. E. Woods, and S. L. Eddins, in *Digital Image Processing Using MATLAB*, 2nd ed. Knoxville, TN, USA: Gatesmark, 2009.
[17] Q. Zhang and I. Couloigner, "Accurate centerline detection and line width estimation of thick lines using the radon transform," *IEEE Trans. Image Process.*, vol. 16, no. 2, pp. 310–316, Feb. 2007.
[18] P. Doucette, P. Agouris, A. Stefanidis, and M. Musavi, "Self-organized clustering for road extraction in classified imagery," *ISPRS-J. Photogramm. Remote Sens.*, vol. 55, no. 5–6, pp. 347–358, Mar. 2001.
[19] C. Ünsalan and B. Sirmaçek, "Road network detection using probabilistic and graph theoretical methods," *IEEE Trans. Geosci. Remote Sens.*, vol. 50, no. 11, pp. 4441–4453, Nov. 2012.
[20] M. Rochery, I. H. Jermyn, and J. Zerubia, "Higher-order active contour energies for gap closure," *J. Math. Imaging Vision*, vol. 29, no. 1, pp. 1–20, Sep. 2007.
[21] A. P. Dal Poz, R. A. B. Gallis, J. F. C. da Silva, and E. F. O. Martins, "Object-space road extraction in rural areas using stereoscopic aerial images," *IEEE Geosci. Remote Sens. Lett.*, vol. 9, no. 4, pp. 654–658, Jul. 2012.
[22] S. Movaghati, A. Moghaddamjoo, and A. Tavakoli, "Road extraction from satellite images using particle filtering and extended Kalman filtering," *IEEE Trans. Geosci. Remote Sens.*, vol. 48, no. 7, pp. 2807–2817, Jul. 2010.
[23] J. Hu, A. Razdan, J. C. Femiani, M. Cui, and P. Wonka, "Road network extraction and intersection detection from aerial images by tracking road footprints," *IEEE Trans. Geosci. Remote Sens.*, vol. 45, no. 12, pp. 4144–4157, Dec. 2007.

[24] C. He, Z. Liao, F. Yang, X. Deng, and M. Liao, "Road extraction from SAR imagery based on multiscale geometric analysis of detector responses," *IEEE J. Sel. Topics Appl. Earth Observ. Remote Sens.*, vol. 5, no. 5, pp. 1373–1382, Oct. 2012.
[25] C. He, F. Yang, S. Yin, X. Deng, and M. Liao, "Stereoscopic road network extraction by decision-level fusion of optical and SAR imagery," *IEEE J. Sel. Topics Appl. Earth Observ. Remote Sens.*, vol. 6, no. 5, pp. 2221–2228, Oct. 2013.
[26] T. Hastie and W. Stuetzle, "Principal curves," *J. Amer. Statist. Assoc.*, vol. 84, no. 406, pp. 502–516, 1989.
[27] U. Ozertem and D. Erdogmus, "Locally defined principal curves and surfaces," *J. Mach. Learn. Res.*, vol. 12, pp. 1240–1286, Apr. 2011.
[28] U. Ozertem and D. Erdogmus, "Principal curve time warping," *IEEE Trans. Signal Process.*, vol. 57, no. 6, pp. 2041–2049, Jun. 2009.
[29] U. Ozertem, "Locally defined principal curves and surfaces," Ph.D. dissertation, Dept. Sci. Eng., Oregon Health Sci. Univ., Portland, OR, USA, 2008.
[30] C. R. Genovese, M. Perone-Pacico, I. Verdinelli *et al.* (2013). *Nonparametric Ridge Estimation* [Online]. Available: http://arxiv.org/pdf/1212.5156v1.pdf.
[31] G. Medioni, M. S. Lee, and C. K. Tang, *A Computational Framework for Segmentation and Grouping.* New York, NY, USA: Elsevier, 2000.
[32] P. Mordohai and G. Medion, *Tensor Voting: A Perceptual Organization Approach to Computer Vision and Machine Learning.* San Mateo, CA, USA: Morgan and Claypool, 2006.
[33] I. Ahamada and E. Flachaire, *Non-Parametric Econometrics.* London, U.K.: Oxford Univ. Press, 2010.
[34] G. Peyré, M. Péchaud, R. Keriven, and L. D. Cohen, "Geodesic methods in computer vision and graphics," *Found. Trends Comput. Graph. Vision*, vol. 5, no. 3–4, pp. 197–397, Mar. 2010.
[35] R. O. Duda, P. E. Hart, and D. G. Stork, in *Pattern Classification*, 2nd ed. New York, NY, USA: Wiley-Interscience, 2001.
[36] C. Wiedemann, C. Heipke, and H. Mayer, "Empirical evaluation of automatically extracted road axes," in *Proc. CVPR Workshop Empirical Eval. Methods Comput. Vision,* Los Alamitos, CA, USA, 1998, pp. 172–187.
[37] VPLab, Downloads. 2013 [Online]. Available: http://www.cse.iitm.ac.in/∼/vplab/satellite.html.

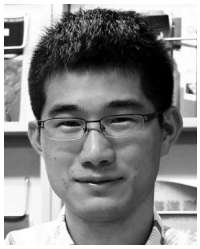

Zelang Miao received the B.S. degree in survey engineering from China University of Mining and Technology, Xuzhou, China, in 2009. He is currently working toward the Ph.D. degree in the Department of Land Surveying and Geo-Informatics, Hong Kong Polytechnic University, Hong Kong, China.

His research interests are image classification and segmentation, pattern recognition, and computer vision methods with applications in remote sensing.

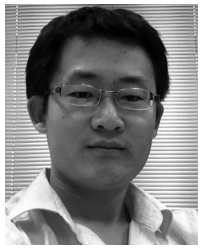

Bin Wang received the B.S. degree in information and computational science from China University of Mining and Technology, Xuzhou, China and the M.Sc. degree in computational mathematics from Dalian University of Technology, Dalian, China, in 2008 and 2011, respectively. He is currently working toward the Ph.D. degree majoring in geographic information science from the Department of Land Surveying and Geo-Informatics, Hong Kong Polytechnic University, Hong Kong, China.

He is the AXA Research Fellow. His current research interests are spatial analysis, mathematical modeling, pattern recognition, etc.

Wenzhong Shi received the Ph.D. degree from University of Osnabrück, Vechta, Germany, in 1994.

He is a Chair Professor in GIS and remote sensing with the Department of Land Surveying and Geo-Informatics, Hong Kong Polytechnic University, Hong Kong, China.

He has published over 100 research papers and 10 books. His current research interests are GIS and remote sensing, uncertainty and spatial data quality control, and image processing for high-resolution satellite images.

Dr. Shi received the State Natural Science Award from the State Council of China in 2007 and the Wang Zhizhuo Award from International Society for Photogrammetry and Remote Sensing in 2012.

Hao Wu received the B.S. and the M.S. degrees from the School of Geodesy and Geomatics, Wuhan University, Wuhan, China and the Ph.D. degree in cartography and GIS from the State Key Laboratory of Information Engineering in Surveying, Mapping, and Remote Sensing, Wuhan University, in 2000, 2003, and 2007, respectively.

He is currently an Associate Professor in the School of Resources and Environmental Engineering, Wuhan University of Technology, Wuhan, China. His research interests are land use change and earth observation science and its applications.